Research Article

Liang Huang*, Yan Cao, Haiyue Zhao, Yufei Li, Yuanfei Wang, and LiRong Wei

Effect of process parameters on density and mechanical behaviour of a selective laser melted 17-4PH stainless steel alloy

https://doi.org/10.1515/phys-2022-0008
received May 18, 2021; accepted November 29, 2021

Abstract: 17-4 PH stainless steel alloy has been widely used in the field of defence industry such as weapon equipment, aerospace, nuclear energy, and so on because of its high strength, high toughness, high temperature resistance, and corrosion resistance. In order to meet the flexible manufacturing requirements of multi-variety small batch complex structure products with lower cost and higher efficiency, selective laser-melted 17-4PH stainless steel alloy has become the focus of research in the field of rapid alloy manufacturing in recent years. In this article, the density characteristics and the distribution characteristics of holes and spheroidization phenomena of 17-4 PH pre-alloyed powder subjected to multidimensional temperature conduction under selective laser melting are studied, and the mechanism of defect generation under temperature conduction is proposed. Finally, the optimal selection of the combination of different process parameters was carried out by orthogonal test, and it was found that the comprehensive mechanical behaviour of the 17-4 PH stainless steel alloy after being formed exceeded the ASTM A564 standard (the yield strength is 1,132 MPa, the tensile strength is 1,323 MPa, and the elongation is 16.6%).

Keywords: selective laser melting, 17-4PH pre-alloyed powder, spheroidization, process parameters, temperature transfer gradient, mechanical behaviour

*** Corresponding author: Liang Huang,** Department of Mechatronic Engineering, Xi'an Technological University, Xi'an 710054, China, e-mail: huangliang@xatu.edu.cn
Yan Cao, Haiyue Zhao, Yufei Li: Department of Mechatronic Engineering, Xi'an Technological University, Xi'an 710054, China
Yuanfei Wang: Tool Structure Manufacturing, Xi'an KunLun Industry (Group) Company with Limited Liability, Xi'an Technological University, Xi'an 710054, China
LiRong Wei: Ministry of Science and Technology, Xi Dian University, Xi'an 710000, China

1 Introduction

As an important member of additive manufacturing (AM), selective laser melting (SLM) has been in the frontier of advanced manufacturing after nearly 30 years of rapid progress. At present, domestic and foreign industrial fields have gradually begun to expand SLM technology for part processing and manufacturing, including aerospace, medicine, common mold manufacturing, and so on. Meanwhile, in the research and development of forming equipment [1,2], technology, and materials, SLM technology has achieved a lot of results. For example, in the actual production process [3,4], the application of this technology to the cemented carbide products with complex-shaped structure can avoid the problems of long period and high cost in traditional cutting methods, and the flexible manufacturing with small batch and multi-variety characteristics can be realized for all kinds of products with complex-shaped structure. As a kind of gun steel material, 17-4PH, due to its excellent strength, corrosion resistance, and toughness, has been widely used in aircraft guns, naval guns, and other military hardware and shows excellent mechanical properties [5], when its working temperature is not more than 500°C. At present, the main traditional processing methods for 17-4PH materials include casting and forging. However, in recent years, in order to adapt to the changing flexible demand of the market, the rapid and precise manufacturing of multi-variety and small-batch complex structure products has gradually become its future development direction, and also challenges the above-mentioned traditional mass quantitative manufacturing modes. Consequently, how to achieve high-efficiency and low-cost flexible manufacturing under the premise of ensuring product quality accuracy and efficiency is the technical bottleneck to be solved and concerned by gun steel manufacturing enterprises in recent years as well. Along with the development of SLM rapid prototyping technology in recent years, more new alloy materials

are developed successfully, and the SLM gun steel materials become possible.

As the SLM technology of this material was introduced recently, related research on SLM forming process of 17-4PH alloy are relatively few. Spierings *et al.* [6] and Gu *et al.* [7] explored the mechanical properties of 17-4 PH powder in the SLM forming process with different process parameters and summarized some laws. Harish, [8] investigated the changes of martensite and austenite of 17-4PH formed parts by changing different protective atmosphere in the forming environment. Based on the aforementioned studies, Rashid *et al.* [9] studied the density and dimensional accuracy of SLM-molded 17-4PH stainless steel with different process parameters. The microstructure and macroscopic mechanical properties of 17-4PH stainless steel formed parts treated with heat treatment and without heat treatment were compared by Professor Gu and his team, and it is considered that heat treatment is helpful for the modification of tissue [10–12].

Based on the aforementioned analyses, it can be seen that although the microstructure and mechanical behaviour of 17-4 PH alloy formed under different process parameters was studied, the measurement of density of 17-4 PH alloy formed by different process parameters was less studied. Therefore, this article selected 17-4 PH stainless steel pre-alloyed powder material to carry out SLM research on EOS M290 forming equipment by exploring 17-4 PH stainless steel powder material rheological characteristic and combining with different process parameters. The effects of the process parameters on the microstructure defects were investigated, and the optimum mechanical properties of the formed parts were obtained by orthogonal test under the condition of the microstructure guarantee. Thus, a theoretical foundation for the preparation of 17-4 PH stainless steel parts with high density and high-performance SLM forming was laid.

2 Experimental

2.1 Selection of 17-4PH pre-alloyed powder

The 17-4 PH pre-alloyed powder components selected in this article meet the ASTM A564 standard. In SLM technology, the structure of pre-alloyed powder affects the quality of forming parts to a certain extent. As the pre-alloyed powder is mostly non-spherical, it will form the material after heating, with powder particles in the process of self-adhesion, and the unadhesive part due to the hot melt forms a bottleneck structure and gradually spheroidizes, and then will gradually melt; and in the process of laser scanning, the stress on the split body of the material will be dispersed in the horizontal and forming directions, and the direct effect of this stress dispersion on the formed part is to warp the formed part. In contrast, the spherical powder material only experiences the process of melting and remelting cooling of the powder during laser irradiation, so the stress produced by laser scanning is rarely dispersed in the horizontal direction, which made the shrinkage volume of the sample less during the forming process, thus avoiding the warping deformation. In this article, the sophericity of 17-4 PH stainless steel pre-alloyed powder was measured and analysed by BT-1600 image particle distributor analysis system, and the distribution of sophericity interval of 17-4 PH stainless steel powder is shown in Table 1 and Figures 1 and 2. As shown above, the pre-alloyed powder was found to be dense and spherical in general, and the dense and smooth powder surface guaranteed good flow characteristics, which were beneficial for the powder feeding process.

Distribution of the particle size of the pre-alloyed powder in a reasonable range will make the powder show good fluidity in the forming process. Correspondingly, the quality of powder laying depends on the fluidity of the material. Good fluidity can make the SLM-formed parts of the material have high quality. In this article, the pre-alloyed powder particle size distribution curve was measured by a Mastersizer laser-diffraction diameter tester (model: ms3000) (as shown in Figure 3). The pre-alloyed powder particle size was in the range of 20–60 μm, and the median particle diameter was 55 μm. Therefore, the selected powder presented a sufficient particle size.

For the characterization of the printability of the selected pre-alloyed powder by rheological characteristic, the material viscosity test (test procedure: prepare 50 mL of deionized water in a beaker then add 8 g pre-alloyed powder to deionized water and stir 2 min with agitator to produce mixed suspension; then, 0.104 g

Table 1: The sophericity distribution of 17-4PH pre-alloyed powder

Maximum sophericity (μm)	Minimum sophericity (μm)	Average sophericity (μm)	Span (μm)
0.999	0.558	0.873	0.161

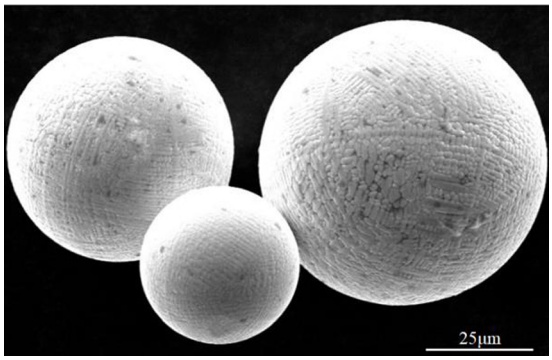

Figure 1: The microstructure of 17-4PH pre-alloyed powder.

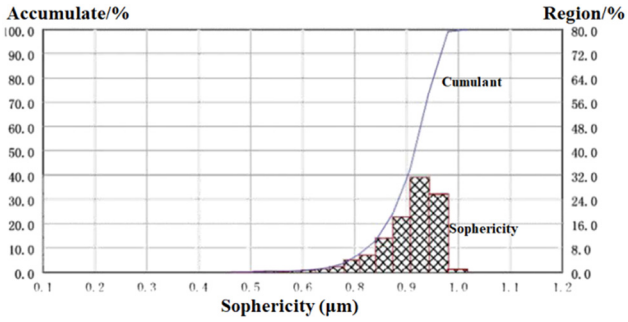

Figure 2: The sophericity distribution of 17-4PH pre-alloyed powder.

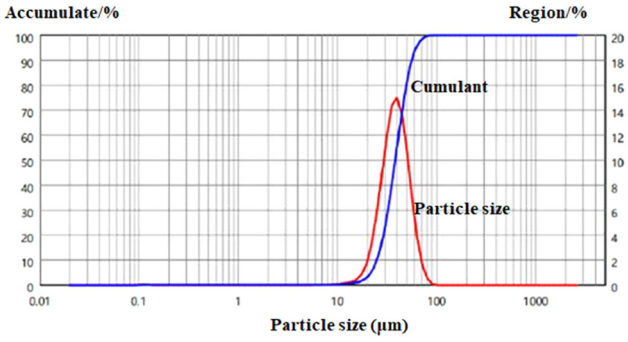

Figure 3: The particle size distribution curve of 17-4PH pre-alloyed powder.

hydroxypropyl methyl cellulose [4,000 viscosity] was added for mixing and stirring for 1 h, and 0.136 g polyethylene imine [M_w = 1,800] was used for bridging flocculation and continued stirring until the mixed solution was uniform, so the 17-4PH pre-alloyed powder suspension mixed samples were obtained for measurement of rheological properties; finally, at room temperature, the viscosity of materials at different time was obtained by changing the shear rate by using a rheometer [model: Anton Paar MCR301], and the results are shown in Figure 4)

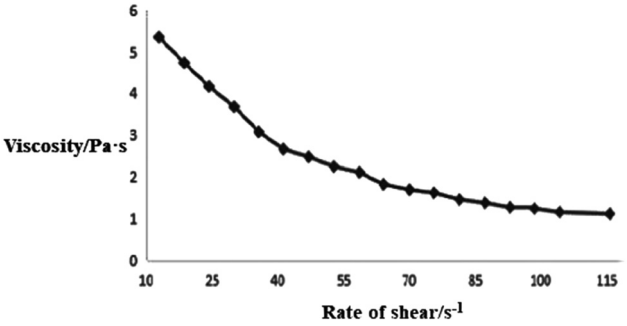

Figure 4: Viscosity curve with shear rate.

was used to characterize the printability of the 17-4 PH pre-alloyed powder. It can be seen that the viscosity of the material will gradually decrease with the increase of the applied shear rate, which reflects the shear viscosity reduction characteristics of the material during this process. 17-4 PH pre-alloyed powder materials show obvious pseudoplastic flow. In the study of pseudoplastic flow materials, the following research formula is used:

$$\eta = K\gamma^{n-1}, \tag{1}$$

where η represents the viscosity of the material, γ represents the size of the shear rate during the experiment, K represents the constant coefficient, and n is the fluidity index of the material, $n < 1$. During the study of the forming properties of metal powder materials, the fluidity index of the material n reflects the degree of the change of the viscosity value of the sample with the shear rate, which is a very critical performance index. It is generally believed that the larger the fluidity index, the less sensitive the viscosity value of the material is to the change of shear rate and the slower the change rate, and the deformation of this material generally has good stability, but the metal powder material in this case does not show sufficient shear thinning behaviour [13–15]. On the basis of this situation, it is proposed that under the premise of $n > 0.2$, the value of n should be as less as possible [16]. This is because the smaller the n, the faster the viscosity of the powder material changes with the shear rate. SLM is carried out rapidly at a certain temperature, so this characteristic of the material is beneficial to the molding of the material. According to formula 1, a double logarithmic diagram of the relationship between sample viscosity and shear rate, that is $\lg\eta$–$\lg\gamma$, is shown in Figure 5. The logarithmic line slope of the material viscosity and shear rate is shown in Figure 6; the value of the epidemic index n of the sample can be calculated, that is $n = 0.2898$, so the material has good SLM forming property [17].

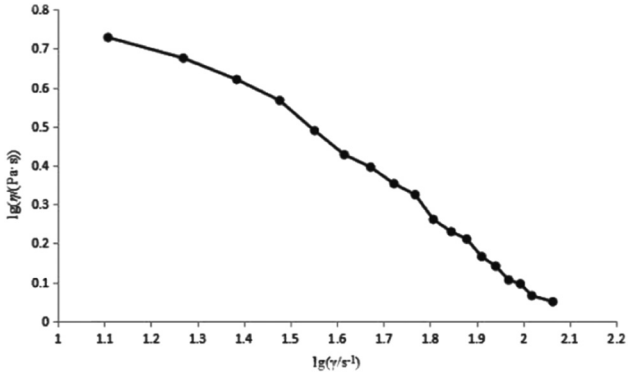

Figure 5: lg η–lg γ relation curve.

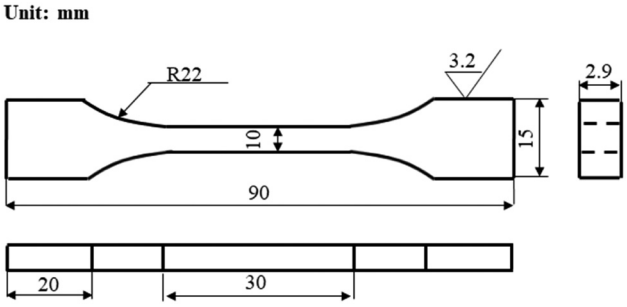

Figure 6: Schematic diagram of the tensile samples.

2.2 Selection of 17-4PH SLM-formed part metallographic equipment

In this experiment, the surface of the sample was polished by using 100#, 240#, and 400# coarse sand in turn, and then polished on the fine sand paper of 800#, 1,000#, 1,500#, 2,000#, and 3,000# in turn. Then, the PG-2D polishing machine (diameter of the polishing wheel is 230 mm, the maximum idle speed is 900 rpm on the left and 700 rpm on the right) is used until there is no obvious scratch on the surface of the sample. After that, the corrosion treatment before the metallographic experiment of the sample is carried out, so that the internal structure of the sample can be observed under the microscope. The corrosion solution used in this experiment is a mixture of 15 mL of glycerin, 10 mL of hydrochloric acid, and 5 mL of nitric acid. The corrosion reaction of the sample is carried out in the corrosion solution or dipped in some corrosion solution for a period of time. The corrosion time can be simply adjusted according to the shape and size of the sample. Finally, the Nicon300 optical microscope, which is equipped with lenses ranging from 50× to 1,000×, is used for easy observation and analysis of samples from different magnification angles.

2.3 Selection of the density measurement method for 17-4PH SLM-formed parts

In this experiment, Archimedes' method is used to measure the density of samples. In order to ensure the accuracy of the experiment, the sample to be tested should be cleaned by an ultrasonic cleaner before the experiment (the solution of the sample to be cleaned is a mixture of acetone and water, and the sample needs to be dried after cleaning), so as to avoid the interference of the residual stains on the surface of the sample to the experimental results. When the measurement begins, an electronic balance is used to weigh the mass of the sample to be measured M_1, then a beaker containing enough distilled water is prepared, and an electronic balance is used to weigh its mass M_2, and then the sample is tied to the beaker slowly. It should be noted that the sample cannot touch the cup wall and bottom of the beaker during the measurement process, otherwise it will affect the experimental results, after the balance is stable, the reading M_3 is recorded at this time. Finally, the density of the sample can be obtained by using formulas (2) and (3).

$$\rho_0 = \frac{M_1\rho_1}{M_3 - M_2}, \tag{2}$$

$$A = \frac{\rho_0}{\rho_2}, \tag{3}$$

where ρ_1 represents the density of water, ρ_0 represents the actual density of the sample, ρ_2 represents the theoretical density sof the sample, and A represents the density.

2.4 Selection of the mechanical behaviour analysis equipment for 17-4PH SLM-formed parts

Tensile test mainly included tensile strength test and yield strength test of the selective laser melted parts. The finished stretch piece must be polished to a surface roughness Ra of 1.6 μm and be used in tensile tests. Before testing, the length of the sample is measured first, and the test parameters are set when stretching: preloading 50 kN and tensile rate 5 mm/min. After the sample is pulled, the data system could provide the corresponding data based on the pre-experiment setting, including the tensile strength (σ_B) and yield strength of the sample (σ_s). Meanwhile, according to the national standard

GB/T 228.1-2010-tensile test of metal materials part 1: room temperature test methods, the tensile samples are shown in Figure 6.

3 Results

3.1 Analysis of density of 17-4PH SLM-formed parts under different process parameters

As the principle of SLM is to melt the pre-alloyed powder by high energy laser beam, the rapid cooling solidification occurs after the laser beam is removed. Therefore, the forming density and quality of the material are mainly restricted by the laser energy of the laser source of the equipment in each formed position and caused by the longitudinal/transverse heat transfer during the sequential sintering between adjacent molten pools/molten channels. In this article, through a large number of forming tests, a set of parameters are selected within the range of process parameters that can be formed (scanning speed: 15–45 mm/min; laser power: 160–220 W; scanning spacing: 9–13 μm), so the forming density under the action of each process parameter is studied by using the control variable method, and the distribution mechanism of material density defect with temperature gradient conduction property is established.

3.1.1 Scanning speed

The laser scanning speed is used to reflect the fixed laser energy time of the pre-alloyed powder in the unit forming area and also reflect the pause time between the two adjacent laser injection points. It is mainly by changing the sintering time in the unit forming area to change the thermal energy of the pre-alloyed powder and acting on the solid-solution aging of the material. This part has taken a certain process parameter as an example (scanning speed: 15–45 mm/min; laser power: 200 W; scanning spacing: 11 μm), and the metallographic phase diagram shown in Figure 7 is obtained by dividing the scanning speed into four stages.

It can be seen from Figure 7 that when the laser power and scanning spacing are fixed as medium parameters, and the scanning speed is higher, the solidification time of the pre-alloyed powder in the unit sintering

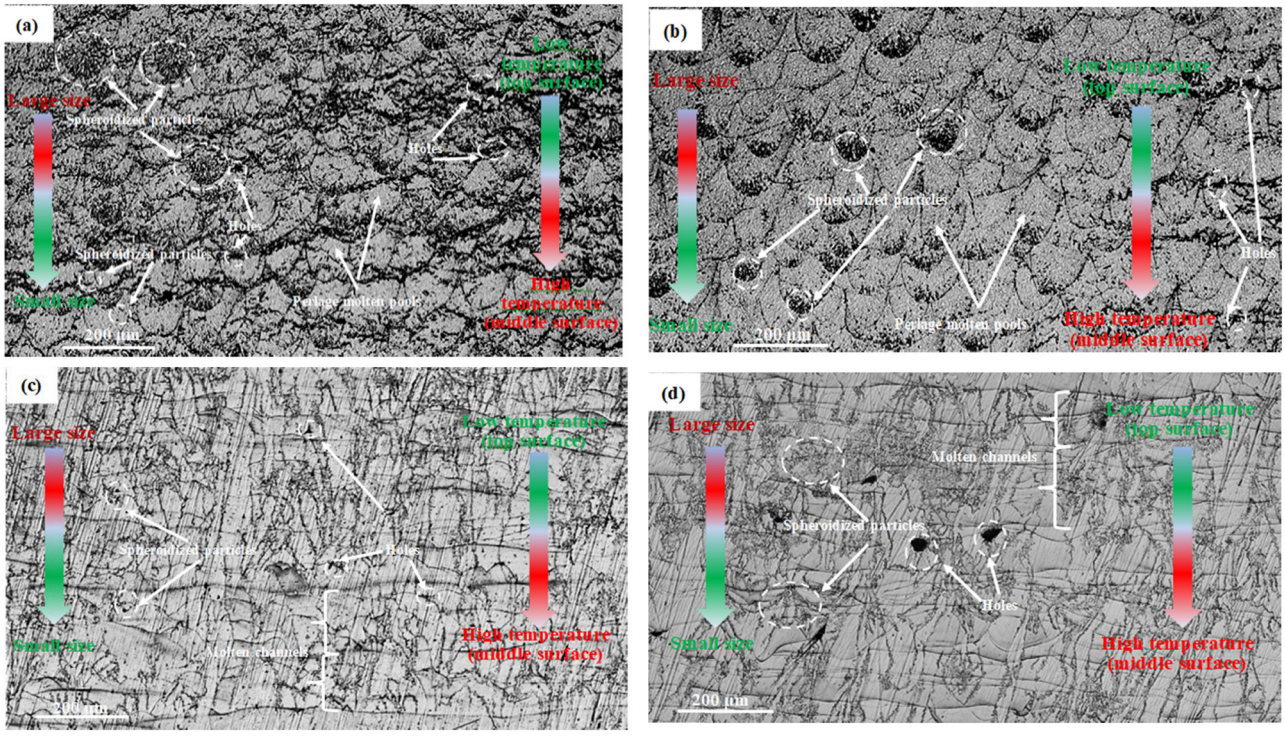

Figure 7: Metallographic phase of samples under different scanning speed: (a) 45 mm/min, (b) 35 mm/min, (c) 25 mm/min, and (d) 15 mm/min.

area is shorter because of the short heating time, and the width size of the molten pools/molten channels is smaller (as shown in Figure 7(a)). Meanwhile, with the decrease of scanning speed, the heat of the pre-alloyed powder in the unit sintering area increases gradually, as a result, Figure 7(b) has a wider-size molten pool structure than Figure 7(a), and Figure 7(d) has a wider-size molten channel structure than Figure 7(c), and the lap quality of the whole material between adjacent molten pools/molten channels decreases gradually, which is mainly reflected in Figure 7(d) as the inconsistency of the width size of adjacent molten channels.

Subsequently, spheroidized particles [18] with small ellipsoidal structure and irregular holes [19,20] with large size were found in each molten pool/molten channel in Figure 7 and showed similar distribution. The reason is that when the scanning speed is high (as shown in Figure 7(a)), on the one hand, the heat produced by the laser source in the unit sintering area is less, so that the pre-alloyed powder in each scanning path cannot be fully sintered and a part of the holes is formed by the powder stacking. On the other hand, considering the short time of solid solution aging, and the liquid vapour produced by the material during melting and the external gas absorbed by the oxide during solidification cannot be eliminated in time due to the high solidification rate in the molten pools/molten channels, thus forming another part of the holes, meanwhile, considering that the bubble solubility increases with the increase of laser energy density during SLM proposed by Xiao *et al.* [21] and the sufficient of powder sintering gradually increased, the holes decrease with the decrease of scanning speed, and at a scanning speed of 25 mm/min to achieve the best (as shown in Figure 7(b) and (c)). The corresponding crystal also has a suitable size in Figure 7(c) (*i.e.* not as small as in Figure 7(b) and as large in Figure 7(d)). However, when the scanning speed is reduced to a certain extent, because the laser energy in the molten pools/molten channels is too high, the scanning width of the corresponding molten pools/molten channels will become larger and the formed part of the previous layer will be secondary melted and heat transferred, as a result, the gas that cannot be discharged in time in the previous layer will be heated and expanded, and finally the hole size becomes larger (as shown in Figure 7(d)). For spheroidization, the formation mechanism is similar to that of holes, which is restricted by temperature transfer. First of all, when the scanning speed is too high in the forming process (as shown in Figure 7(a)), the pre-alloyed powder in the forming layer cannot be completely melted, in addition, when the molten liquid metal flows under the coupling of its surface tension and solidification gradient, and the liquid metal meets the unmelted solid powder particles, the liquid metal will be coated in the outer layer of its surface, and when the laser movement occurs rapid cooling to form spheroidized particles, due to more spheroidized particles are produced at this time, so larger size spheroidized particles will be formed by annexation (as shown in Figure 7(a)). In the process of increasing the scanning speed gradually (as shown in Figure 7(b) and (c)), the pre-alloyed powder absorbs more energy, so it transforms more powder into molten metal, thus reducing the spheroidization. However, when the scanning speed is reduced to a certain extent, the excessive laser energy will accelerate the gasification rate of liquid metal, and the smaller spheroidized particles will be attached to the forming layer by vapourization rising and solidification (as shown in Figure 7(d)). In addition, considering that the temperature gradient direction in the molten pools is longitudinal along the forming direction, while the temperature gradient direction in the molten channels is the radial direction of sintering in turn, this will lead to spheroidization and holes in each molten pool mainly concentrated at the bottom of the lower temperature, while spheroidization and holes in the molten channel are mainly concentrated on both sides of the boundary of the lower temperature, and generally all decrease along the temperature gradient, and the corresponding temperature gradient determines the size and quantity of spheroidization and holes, so the distribution of spheroidization and hole along the temperature gradient can be observed in Figure 7.

3.1.2 Laser power

Laser power is the key process parameter which directly affects the density and quality of SLM-formed parts. Its size directly determines the heat energy of the unit forming area of the pre-alloyed powder in unit time and is finally reflected in the solid-solution aging process of the material. Through the analysis of the above scanning speed, it can be seen that the scanning speed is mainly by changing the sintering time in the unit forming area to change the thermal energy of the pre-alloyed powder and acting on the solid-solution aging of the material. Therefore, the influence mechanism of these two parameters on the density of materials is consistent. Based on the above forming process parameter range and the best scanning speed parameters (scanning speed: 25 mm/min; laser power: 160–220 W; scanning spacing: 11 μm), the metallographic phase diagram shown in Figure 8 is obtained by dividing the laser power into four stages.

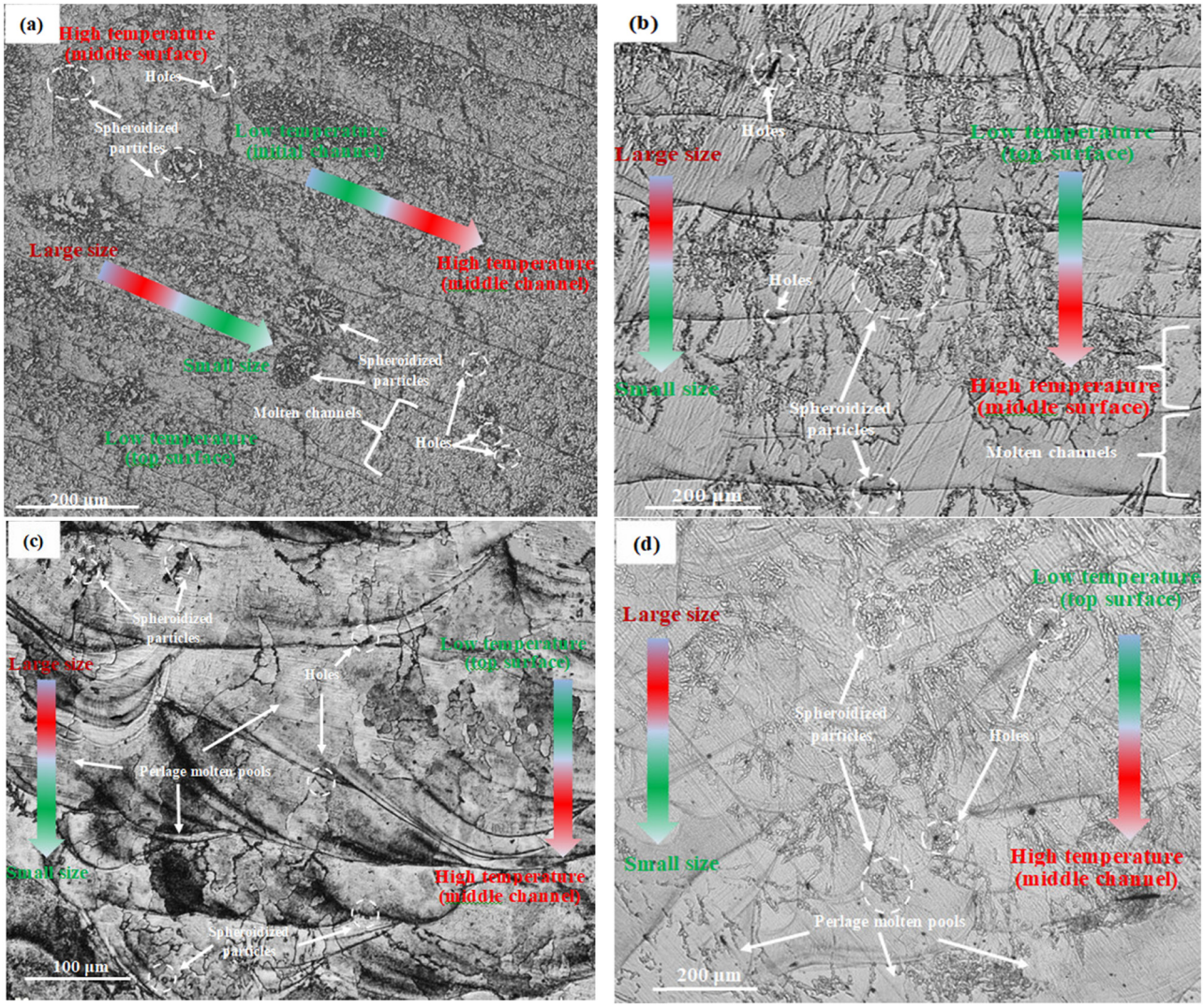

Figure 8: Metallographic phase of samples under different laser power: (a) 160 W, (b) 180 W, (c) 200 W, and (d) 220 W.

It can be seen from Figure 8 that when the scanning speed and scanning spacing are fixed as medium parameters, and the laser power is lower (as shown in Figure 8(a)), all the pre-alloyed powders on the forming layer cannot absorb enough heat and hence most of the powder inside the forming layer cannot be fully melted, and the temperature gradient in the forming layer is small, and so the forming layer shows the phenomenon that the radial molten channel width is small and the adjacent channel spacing is large and the longitudinal "perlage" molten pool width is small and the length is long due to the small surface tension of liquid metal and the shear stress of solidification phase boundary coupling (*i.e.* Marangoni flow). Meanwhile, with the increase of laser power, the thermal energy of the pre-alloyed powder in the forming layer is high enough to fully melt, and the surface tension inside the liquid metal is improved, so that the radial width of the molten channel and the "perlage" molten pool is reasonably expanded, and the longitudinal length of the molten pool decreases gradually and eventually develops from length to width (as shown in Figure 8(b) and (c)). However, when the laser power is higher than the appropriate range, the pre-alloyed powder on the forming layer will have higher fluidity due to the excessive absorption of laser energy and cover the adjacent formed layer and the galvanized layer, which result in the different width of each molten pool and molten channel (as shown in Figure 8(d)).

Subsequently, it can be seen from Figure 8(a) that when the laser power is low, the pre-alloyed powder absorbs less energy per unit time in the forming area, so most of the pre-alloyed powder in the forming area is not fully melted and a large number of spheroidization

and holes are formed in the molten channels and molten pools. Meanwhile, as the temperature in the forming layer is transferred from the top to the bottom, the forming layer closer to the middle shows less holes and spheroidization than the top of the forming layer because of more heat energy. For the distribution of holes and spheroidization in the same forming layer (*i.e.* the initial section of the molten channels is higher than that of the middle section of the molten channels), the cause is the same. In addition, the larger size spheroidization and holes are still concentrated at the boundary of the molten pool/molten channel due to the conduction of temperature gradient. Then, the spheroidization and holes decrease with the increase of laser power, and at a laser power of 200 W the best is achieved (as shown in Figure 8(b) and (c)). However, when the laser power is higher than the reasonable range, because the energy obtained by the pre-alloyed powder in the forming area is too high per unit time, on the one hand, the radial width of the molten pool and the molten channel is increased and the boundary secondary remelting makes the arrangement of the molten pool and molten channel disordered. On the other hand, due to the remelting of the formed molten channel and molten pool, the phenomenon of holes and spheroidization in the formed layer increases, and because of the conduction of longitudinal temperature gradient, there are fewer defects in the middle of the formed layer than in the top/bottom surface (as shown in Figure 8(d)).

3.1.3 Scanning spacing

The scanning spacing refers to the centre distance of the laser source between the two adjacent scanning paths, which affects the forming quality and density by acting on the lap rate (the ratio of the lap width of the molten channel to the whole width of the molten channel) between the adjacent molten pool/molten channel. The lap rate (as shown in Figure 9) of molten pool/molten channel is generally calculated by formula (4). Based on the above forming process parameter range and the best scanning speed parameters and best laser power (scanning speed: 25 mm/min; laser power: 200 W; scanning spacing: 9–13 μm), the metallographic phase diagram shown in Figure 10 is obtained by dividing the laser power into three stages.

$$\eta_l = \frac{D_w}{W} \cdot 100\% = \frac{W - S}{W} \cdot 100\% = \left(1 - \frac{S}{W}\right) \cdot 100\%, \quad (4)$$

where D_w represents the lap width, W represents the scanning width, and S represents the scanning spacing.

It can be seen from Figure 10 that when the scanning speed and laser power are fixed as medium parameters, and the scanning spacing is higher (as shown in Figure 10(a)), according to formula (4), the overlap width (D_w) between adjacent channels is very small, and the pre-alloyed powder at the boundary of molten pool/molten channel will be difficult to form a better metallurgical connection and formed a more obvious depression morphology because of the less heat transfer of adjacent formed parts (as shown in Figure 10(a)). With the decrease of scanning spacing, the lap rate of the molten channel/molten pool increases gradually, which makes the pre-alloyed powder at the boundary of the molten pool/molten channel receive good heat transfer of the adjacent formed parts and have excellent metallurgical connection characteristics (as shown in Figure 10(b)). When the scanning spacing is reduced to a certain extent, because the lap rate of the molten channel/molten channel is too high, it is easy to remelt the pre-alloyed powder by the high heat transfer of the adjacent molten channel/molten channel under the irradiation of certain intensity laser source parameters, and when it is heated too much, it will expand, resulting in the surface of the forming layer prone to bulge phenomenon (as shown in Figure 10(c)).

Subsequently, as the laser source energy of this forming mode of SLM has Gaussian distribution properties (as shown in Figure 11, *i.e.* from the radial

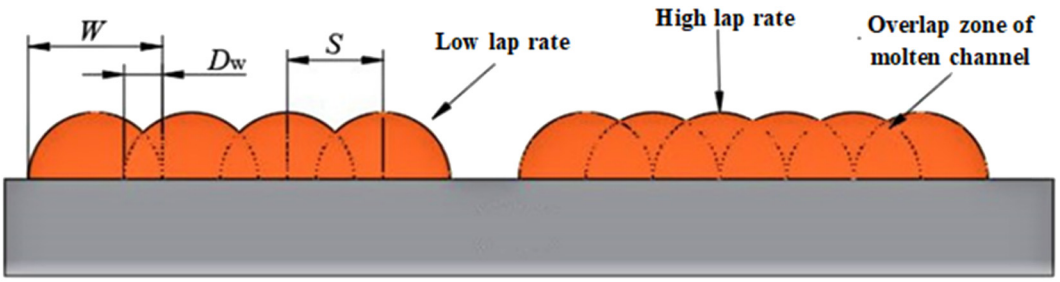

Figure 9: Diagrammatic sketch of scanning spacing.

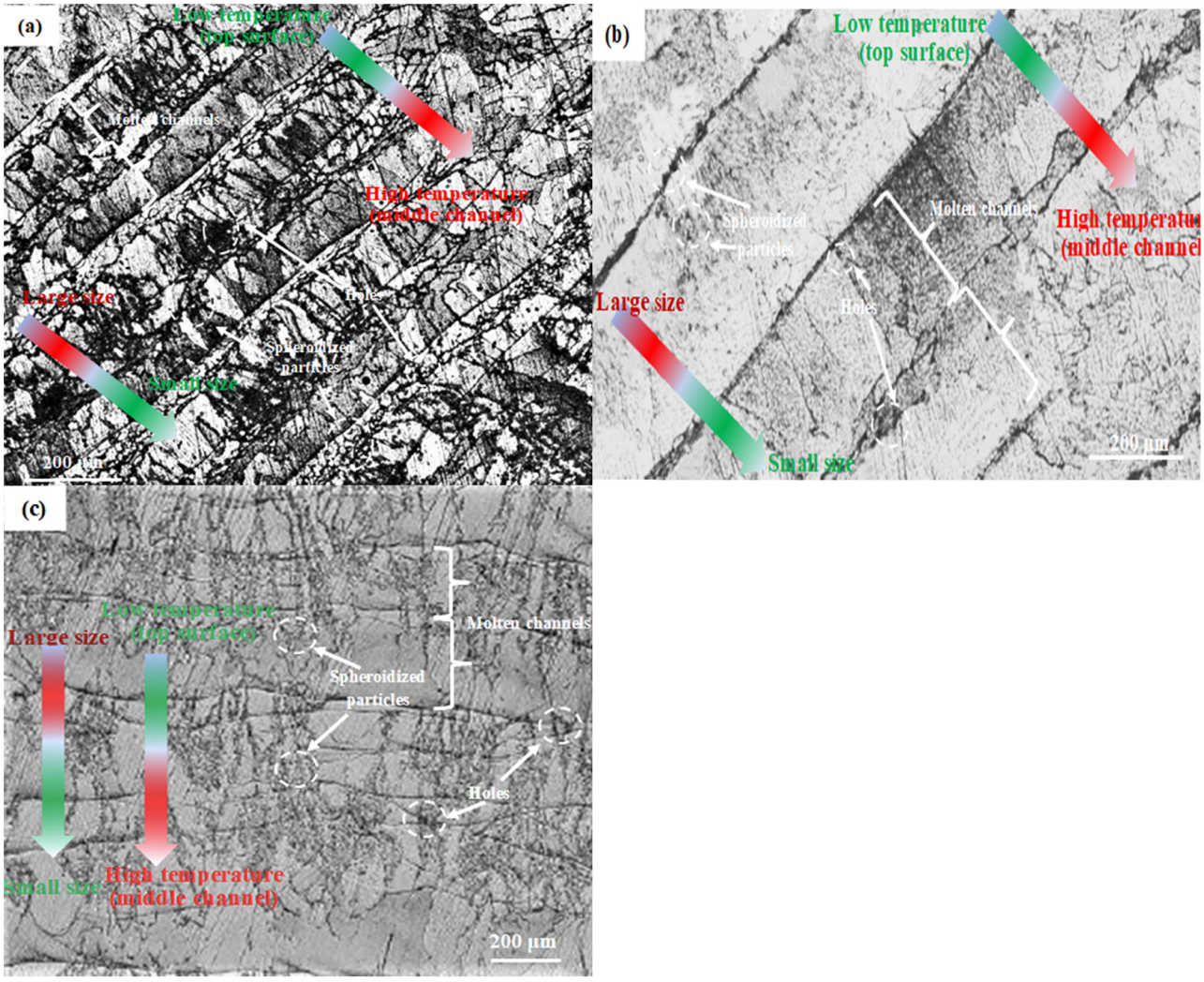

Figure 10: Metallographic phase of samples under different scanning spacing: (a) 13 μm, (b) 11 μm, and (c) 9 μm.

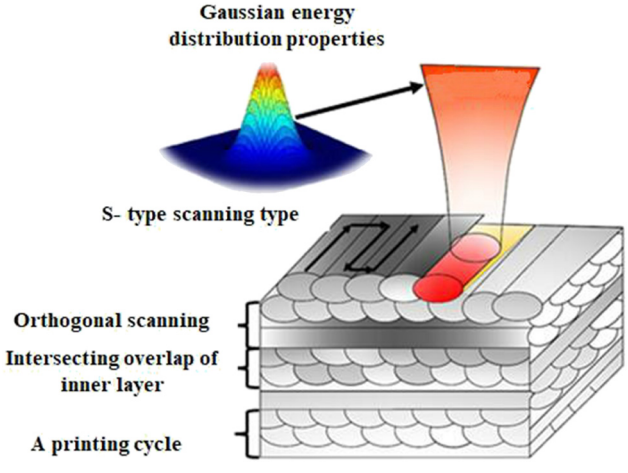

Figure 11: Schematic diagram of scanning method.

perspective, the energy of the laser centre is higher than the energy on both sides), the energy obtained at the molten channel boundary is less relative to the middle part of the molten channel, so it can be seen from Figure 10(a) that when the scanning spacing is high, the pre-alloyed powder on the molten pool/molten channel boundary absorbs less energy, so a large number of holes and spheroidization will be produced by obtaining less heat transfer of adjacent formed layers at the boundary of the molten pool/molten channel. With the decrease of scanning spacing, the overlap width of the molten channel/molten pool increases due to the decrease of scanning spacing, so that the pre-alloyed powder in the boundary region is properly remelted by sufficient heat. Thus, the above holes and spheroidization are greatly improved (as shown in Figure 10(b)). When the scanning spacing is reduced to a certain extent, the pre-alloyed powder at the boundary of

Table 2: Measurement results of sample density under different process parameters

Scanning speed (mm/min)	Laser power (W)	Scanning spacing (μm)	Density (%)	Vickers hardness (HV)
45	**200**	**11**	**86.1**	**340**
35	200	11	94.9	404
25	**200**	**11**	**98.4**	**431**
15	200	11	96.7	418
25	**160**	**11**	**90.8**	**376**
25	180	11	95.3	409
25	**200**	**11**	**98.9**	**439**
25	220	11	97.2	425
25	**200**	**13**	**91.4**	**383**
25	**200**	**11**	**99.4**	**441**
25	200	9	96.9	423

The bold form shows the extremum of the mechanical properties in each group of control variables method.

the molten pool/molten channel receives higher heat from the adjacent formed part. Therefore, the boundary part will increase the phenomenon of holes and spheroidization by a higher degree of remelting, and the distribution trend is consistent with the direction of temperature gradient (as shown in Figure 10(c)). Meanwhile, on the one hand, the Gaussian energy characteristic distribution of laser sources will increase the thermal energy of the molten channel boundary compared to the intermediate deficiency; on the other hand, even if the repeated accumulation of the molten channel boundary allows it to obtain more energy and melt, because the energy is still not very high and for considering the melting tissue in the middle part, the optimal parameter can only minimize the spheroidization in the gap and not completely eliminated.

Finally, the density of the samples under the above process parameters is characterized by Archimedes' method, and the measurement results are obtained as shown in Table 2. It can be seen that the relationship between holes and spheroidization is proportional to the density of the SLM-formed parts, and the density is proportional to the hardness of the material, in which the density and hardness reach the highest (99.4%, 441HV) when the laser power is 220 W, the scanning speed is 25 mm/min, and the scanning spacing is 11 μm.

3.2 Analysis of optimal process parameters of 17-4PH SLM-formed parts

In the previous study of the influence of several different main parameters on the microstructure, density, and hardness of the formed parts, the local optimal process parameters were obtained. In this experiment, we mainly studied the mechanical properties of the molded parts under different parameter arrays under normal temperature and static load tensile test by orthogonal test. In order to obtain the global optimal forming process parameters, the adjustable range of the parameters of the forming equipment is divided into three levels: high, low, and high (as shown in Table 3), and the tensile properties of each sample are evaluated by orthogonal test [22].

It can be seen from the orthogonal test results that the samples 1#, 5#, 9# all have high tensile properties. Furthermore, the elongation of these three groups of parameters was compared and found that when the laser power is 200 W, the scanning speed is 25 mm/min, and the scanning spacing is 11 μm, the highest mechanical properties were present (*i.e.* the yield strength is 1,132 MPa, the tensile strength is 1,323 MPa, and the elongation is 16.6%). Therefore, it can be seen that the mechanical behaviour of the 17-4 PH

Table 3: Orthogonal test results

Group number	Impact factors			Mechanical properties		
	Laser power (W)	Scanning speed (mm/min)	Scanning spacing (μm)	σ_s (MPa)	σ_B (MPa)	δ (MPa)
1	180	15	9	1,127	1,317	16.3
2	180	25	11	1,089	1,169	15.6
3	180	35	13	1,027	1,089	14.7
4	200	15	9	1,107	1,217	11
5	**200**	**25**	**11**	**1,132**	**1,323**	**16.6**
6	200	35	13	1,043	1,198	15.9
7	220	15	9	1,076	1,288	15.8
8	220	25	11	1,108	1,305	14.9
9	220	35	13	1,115	1,321	16.1

The bold from shows the optimal values for the mechanical properties in each group of control variable methods.

alloy sintered by selective laser melted is much higher than that of the ASTM A564 criteria (σ_s > 1,000 MPa, σ_B > 1,000 MPa, δ > 12%).

4 Conclusion

As the principle of SLM is to melt the pre-alloyed powder by high energy laser beam, the rapid cooling solidification occurs after the laser beam is removed. Therefore, the forming density and quality of the material are mainly restricted by the laser energy of the laser source of the equipment in each formed position and caused by the longitudinal/transverse heat transfer during the sequential sintering between adjacent molten pools/molten channels. In this article, the control variable method and the orthogonal test method are used to study and analyse the related process parameters, and it is found that:

1) The laser scanning speed, laser power, and scanning spacing are all changed by changing the absorption heat state of the pre-alloyed powder in the scanning path to change the solid-solution aging process of the material so as to affect the forming density and forming quality. Furthermore, the laser scanning speed changes the heat energy of the prealloy powder mainly by changing the sintering time of the unit-formed region, the laser power directly determines the heat energy of the unit forming area of the pre-alloyed powder in unit time, and the scanning spacing mainly determines the absorption heat energy of the pre-alloyed powder at the boundary of the molten pool/molten channel.

2) Because the pre-alloyed powder has different thermal energy under different process parameters, it is easy to form the spheroidized particles with small ellipsoidal structure and irregular holes with large size at the boundary position of the molten channels/molten pools under the longitudinal/transverse multidimensional heat conduction between adjacent molten channels/molten pools, and the distribution mode (size from large to small and quantity from large to small) is consistent with the direction of temperature gradient.

3) The density of the 17-4PH stainless steel alloy is proportional to the size and quantity of the holes and spheroidization in the formed layer, while the density of the material is related to the macroscopic hardness and tensile properties. And the mechanical behaviour of selective laser melted 17-4 PH alloy (the yield strength is 1,132 MPa, the tensile strength is 1,323 MPa, and the elongation is 16.6%) is higher than ASMT A564 standard by using the optimal parameters obtained by orthogonal test.

Funding information: This research was funded by National Natural Science Foundation of China (NSFC) under grant number 51705392 and the project of 2019 Yulin Science and Technology Program under grant number K20190176.

Author contributions: Liang Huang and Yan Cao: methodology; Ruochen Zhao: validation; Liang Huang, Haiyue Zhao, and Yunpeng Dang: formal analysis; Liang Huang and Yao Li: investigation; Yunpeng Dang: resources; Yuanfei Wang: writing, original draft preparation; Liang Huang and Yan Cao: writing, review, and editing; Liang Huang: project administration; Yan Cao and Yuanfei Wang: funding acquisition. All authors have accepted responsibility for the entire content of this manuscript and approved its submission.

Conflict of interest: The authors state no conflict of interest.

Data availability statement: All data included in this study are available upon request from the corresponding author.

References

[1] Brighenti R, Cosma MP, Marsavina L, Spagnoli S, Terzano M. Laser-based additively manufactured polymers: a review on processes and mechanical models. J Mater Sci. 2021;56:961–98. doi: 10.1007/s10853-020-05254-6.

[2] Razavykia A, Brusa E, Delprete C, Yavari R. An overview of additive manufacturing technologies-a review to technical synthesis in numerical study of selective laser melting. Materials. 2020;13:93–6. doi: 10.3390/ma13173895.

[3] Stolt R, Elgh F. Introducing design for selective laser melting in aerospace industry. J Computdes Eng. 2020;7:489–97. doi: 10.1093/jcde/qwaa042.

[4] Zhang L, Song B, Fu JJ, Wei SS, Shi YS. Topology-optimized lattice structures with simultaneously high stiffness and light weight fabricated by selective laser melting: design, manufacturing and characterization. J Manuf Process. 2020;56:1166–77. doi: 10.1016/j.jmapro.2020.06.005.

[5] Yu ZY, Zheng Y, Chen JM, Wu CF, Xu JJ, Lu H, et al. Effect of laser remelting processing on microstructure and mechanical properties of 17-4 PH stainless steel during laser direct metal deposition. J Mater Process Tech. 2020;284:1–13. doi: 10.1016/j.jmatprotec.2020.116738.

[6] Spierings AB, Schoepf M, Kiesel R. Optimization of SLM productivity by aligning 17-4PH material properties on part

requirements. Rapid Prototyping J. 2013;20:444–8. doi: 10.1108/RPJ-04-2013-0045.
[7] Gu HF, Gong HJ, Pa DP, Rafi K, Stucker K. Influences of energy density on porosity and microstructure of selective laser melted17-4PH stainless steel. Proc Annu Int Solid Freeform Fabrication Symposium-An Additive Manufact Conf. 2016;25:411–7, https://www.researchgate.net/publication/280114488_Influences_of_Energy_Density_on_Porosity_and_Microstructure_of_Selective_Laser_Melted_17-4PH_Stainless_Steel.
[8] Harish I, John SDJ, Somayeh P, Sunil B, Jason S, Kunal K, et al. Effects of particle characteristics on the microstructure and mechanical properties of 17-4 PH stainless steel fabricated by laser-powder bed fusion. Mater Res Technol. 2018;331:192–203. doi: 10.1016/j.powtec.2018.03.025.
[9] Rashid R, Masood SH, Ruan D, Palanisamy S, Rahman Rashid RA, Brandt M. Effect of scan strategy on density and metallurgical properties of 17-4PH parts printed by selective laser melting (SLM). J Mater Process Tech. 2017;249:502–11. doi: 10.1016/j.jmatprotec.2017.06.023.
[10] Veliolu Z. Soluble product of parafree lie algebras and its residual properties. Appl Math Nonlinear Sci. 2020;5:509–14. doi: 10.2478/amns.2019.2.00036.
[11] Shi K, Tang YY, Zhong SM, Yin C, Huang XG, Wang WQ. Nonfragile asynchronous control for uncertain chaotic Lurie network systems with Bernoulli stochastic process. Int J Robust Nonlin. 2018;28:1693–714. doi: 10.1002/rnc.3980.
[12] Long GX, Shi X, Ping L, Jie Z. Study on formation of selective laser melted 17-4 PH alloy. Mech Eng. 2017;2:69–71. doi: 1002-2333(2017)02-0069-03.
[13] Medvedeva MA, Simos TE, Tsitouras CH. Sixth-order, P-stable, Numerov-type methods for use at moderate accuracies. Math Methods Appl Sci. 2021;44:1–10. doi: 10.1002/mma.7233.
[14] Wu JZ, Yuan JB, Gao W. Analysis of fractional factor system for data transmission in SDN. Appl Math Nonlinear Sci. 2019;4:191–6. doi: 10.2478/AMNS.2019.1.00025.
[15] Medvedev MA, Simos TE, Tsitouras C. Explicit, eighth-order, four-step methods for solving inhomogeneous linear problems X”(T) = Lambda X(T) Plus F(T). Bull Malaysian Math Soc Ser. 2019;42:2025–32. doi: 10.1007/s40840-019-00879-6.
[16] Gill SS, Kaplas M. Efficacy of powder-based three-dimensional printing (3DP) technologies for rapid casting of light alloys. Int J Adv Manuf Tech. 2011;52:53–64. doi: 10.1007/s00170-010-2716-1.
[17] Sayanjali M, Rezadoust AM, Sourk FA. Tailoring physico-mechanical properties and rheological behavior of ABS filaments for FDM via blending with SEBS TPE. Rapid Prototyping J. 2020;26:1–5. doi: 10.1108/RPJ-06-2019-0173.
[18] Lee HJ, Dao VH, Ma YW, Yu JM, Yoon KB. Effects of process parameters on the high temperature strength of 17-4PH stainless steel produced by selective laser melting. J Mech Sci Technol. 2020;34:3261–72. doi: 10.1007/s12206-020-0718-y.
[19] Zhao CH, Li JY. Equilibrium selection under the Bayes-based strategy updating rules. Symmetry. 2020;12:739. doi: 10.3390/sym12050739.
[20] Huang R, Dai N, Cheng XS, Wang L. Topology optimization of lattice support structures for heat conduction in selective laser melting. Int J Adv Manuf Tech. 2020;109:1841–51. doi: 10.1007/s00170-020-05741-9.
[21] Xiao R, Yang W, Kai C. Porosity characterization in laser welds of Al-Li alloy 1420. Appl Laser. 2007;27:13–7. doi: 10.3969/j.issn.1000-372X.2007.01.004.
[22] Wan L, Xia ZX, Song Y, Zhang X, Shi S. Parameter optimization of selective laser melting fabricated titanium alloy using skin-core and triple contour scanning strategy. J Laser Appl. 2020;32:15–20. doi: 10.2351/7.0000180.